

# Heterogeneous Graph-based Knowledge Transfer for Generalized Zero-shot Learning

Junjie Wang\*, Xiangfeng Wang<sup>†</sup>, Bo Jin<sup>‡</sup>, Junchi Yan<sup>§</sup>, Wenjie Zhang<sup>¶</sup> and Hongyuan Zha<sup>||</sup>

November 21, 2019

## Abstract

Generalized zero-shot learning (GZSL) tackles the problem of learning to classify instances involving both seen classes and unseen ones. The key issue is how to effectively transfer the model learned from seen classes to unseen classes. Existing works in GZSL usually assume that some prior information about unseen classes are available. However, such an assumption is unrealistic when new unseen classes appear dynamically. To this end, we propose a novel heterogeneous graph-based knowledge transfer method (HGKT) for GZSL, agnostic to unseen classes and instances, by leveraging graph neural network. Specifically, a structured heterogeneous graph is constructed with high-level representative nodes for seen classes, which are chosen through Wasserstein barycenter in order to simultaneously capture inter-class and intra-class relationship. The aggregation and embedding functions can be learned through graph neural network, which can be used to compute the embeddings of unseen classes by transferring the knowledge from their neighbors. Extensive experiments on public benchmark datasets show that our method achieves state-of-the-art results.

## 1 Introduction

Zero-Shot Learning (ZSL) that can handle samples falling into unseen categories has recently received intensive attention [23, 36, 33]. The key challenging problem of ZSL is how one can correctly classify those instances from unseen classes which are absent during training? In general, the instances can be described by some common high-level semantic information, for instance the pattern, color and shape in Fig. 1. One viable approach to deal with the unseen classes is to transfer knowledge learned from seen classes exploring those common semantic information mentioned above. Following this approach, the success of ZSL in general depends on the following two factors: (1) how to capture relationship between all seen and unseen classes? (2) how to transfer knowledge based on this relationship?

Effective modeling of the relationship is of vital importance to knowledge transfer, which has been intensively studied in literature. One typical way is to use the high-level semantic information to bridge seen classes and unseen ones. The attribute vector for each class is usually called **class**

---

\*School of Computer Science and Technology, East China Normal University, Shanghai 200092, China. (E-mail: jasonwang.ecnu@gmail.com)

<sup>†</sup>School of Computer Science and Technology, East China Normal University, Shanghai 200062, China. (E-mail: xfwang@cs.ecnu.edu.cn)

<sup>‡</sup>School of Computer Science and Technology, East China Normal University, Shanghai 200062, China. (E-mail: bjin@cs.ecnu.edu.cn)

<sup>§</sup>Department of Computer Science and Engineering, Artificial Intelligence Institute, Shanghai Jiao Tong University, Shanghai 200240, China. (E-mail: yanjunchi@sjtu.edu.cn)

<sup>¶</sup>Tecent, Shenzhen 518000, China. (E-mail: izhangwenjie@gmail.com)

<sup>||</sup>School of Computer Science and Technology, East China Normal University, Shanghai 200062, China. (E-mail: zha@cs.ecnu.edu.cn)

**prototype**, It is one of the most widely used semantic information to construct the relationship. For example, in prototypical network [28], the visual features are directly mapped into attribute space, and the nearest class prototype is selected as its label. However, these approaches only introduce the same semantic space to represent both seen and unseen classes without capturing relationship explicitly. Another way is to construct relationship explicitly by using knowledge graph (KG) [16]. Nevertheless, unseen class information is required to construct the graph before training, hence the model need to be retrained every time a new unseen class appears.

In this paper, we propose a novel and explainable way to utilize the relationship between seen and unseen classes for ZSL. In particular, we address a more realistic scenario, which involves the inference of both seen and unseen classes at testing phase — generalized zero-shot learning (GZSL). Furthermore, our method is agnostic to both unseen images and unseen semantic vectors during training phrase, thus enjoying more flexibility in practice compared with many previous methods [34, 16].

To this end, we construct a graph with heterogeneous structure to capture intra-class and inter-class relationship simultaneously, each node representing one instance. In order to capture intra-class relationship, we construct a complete graph for all the instances in each class, which can force instances to be as close as possible in embedding space. More importantly, more similar classes should be closer in embedding space, thus we also need to construct inter-class relationship for transferring knowledge between classes. However, there are many instances in each class, thus it is essential to select representative nodes to represent the whole class. Inspired by Generative Adversarial Networks (GAN) [12], the instances belonging to the same class are expected to be subject to the same distribution. As a result, the normalized feature vector of each instance can be considered as a discrete vector sampled from this common distribution. The Wasserstein metric [31] is a natural measure of probability distribution. Thus the representative node of each class is selected as the one nearest to the barycenter, while the distance is defined by the Wasserstein metric. All the seen classes are connected by linking these representative nodes following kNN scheme. Based on the intra-class and inter-class connections, we obtain the heterogeneous graph with two node types on the seen classes as shown on the left of Fig. 2.

Another important issue is to transfer knowledge based on the well-constructed heterogeneous graph. We focus on transferring intra-class and inter-class knowledge simultaneously. Two problems need to be solved, i.e., which embedding space to choose and how to technically transfer information on the graph. Most existing models choose either the semantic space or an intermediate space as embedding space, which usually lead to the so-called hubness problem [27], i.e., there always exist some points which are 'universal' neighbors or hubs for most of all other points. To alleviate this problem, we use the output visual feature space as the embedding space. Moreover, the popular graph neural network (GNN) is utilized to transfer knowledge rely on the heterogeneous graph, which maintains the topology in embedding space. Especially, the aggregation and embedding functions are calculated by using seen training data, further we can obtain the embedding expression of new unseen classes by aggregating their neighbors. The general algorithm framework can be found in Fig. 2.

To summarize, we propose an effective, practical and explainable GZSL algorithm with key contributions as: 1) We capture inter-class and intra-class relationship jointly by constructing a heterogeneous structured graph; 2) Instead of averaging instances directly, we utilize Wasserstein

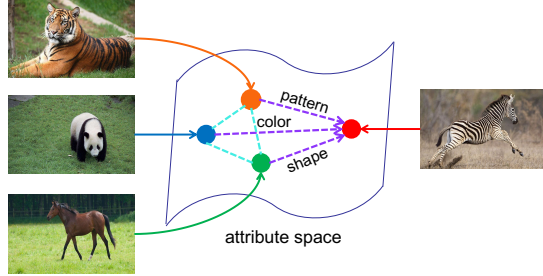


Figure 1: The unseen class in training set (zebra) and seen classes (tiger, panda and horse) can be described by common semantic information (attribute: pattern, color and shape).

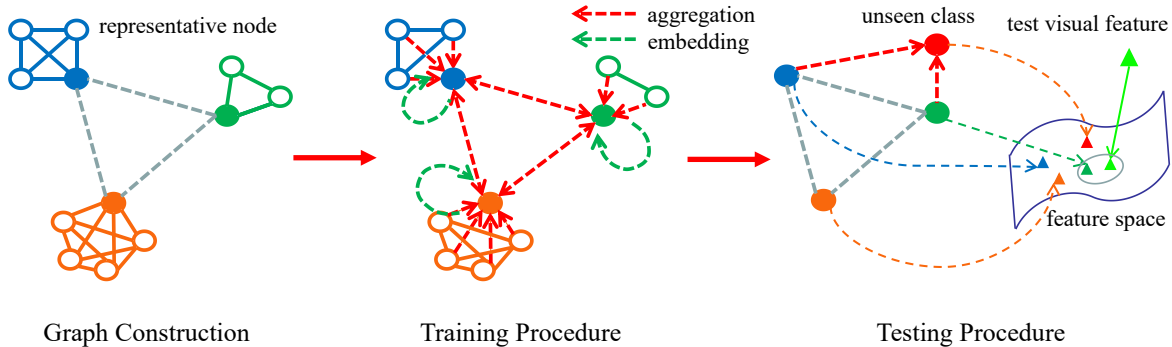


Figure 2: Pipeline of our approach. Left: each class corresponds to a complete graph and all complete subgraphs are connected based on their representative nodes (solid circle). Middle: the embedding vector of representative nodes are produced by both aggregation and embedding functions which is agnostic to to unseen class. Right: connect the new unseen class with  $k$ -nearest seen classes in visual feature space; select the nearest class by visual feature distance as the prediction for each test sample.

metric to extract more representative node of each class; 3) Our approach is the novel inductive GNN-based GZSL method that is agnostic to unseen information during training. Knowledge is transferred from seen classes to new unseen classes based on the learned aggregation and embedding functions.

## 2 Related Work

There has recently been intensive works on generalized zero-shot learning. Most works rely on side information such as attributes to establish connection [11]. Based on these well-defined attributes, traditional algorithms establish the bridge between visual features and class prototype. These approaches can be viewed from the perspective of embedding space and embedding model.

### 2.0.1 Embedding Space.

One of the most intuitive embedding space is the semantic space, i.e., mapping the feature space directly into attributes space. The work [19] proposes Direct Attribute Prediction (DAP) and Indirect Attribute Prediction (IAP) respectively, which both learn the mapping from visual feature space to attribute space via support vector machine (SVM).

Another popular way is to map both features and attributes into an intermediate space. The authors in [38] consider each source or target data sample as a mixture of seen class proportions, and moreover it's natural to map features and attributes into the simplex of seen classes by measuring similarity. Many algorithms are devised following this direction, e.g., [26, 37].

Another line of research is to oppositely embed attributes into the visual feature space. The work [27] demonstrates the existence of some ‘universal’ neighbors or hubs, which indicates that kNN based methods would suffer from the hubness problem. The work [20] shows how to embed attributes into the visual feature space inductively, which can mitigate both hubness problem.

### 2.0.2 Embedding Model.

From the perspective of embedding modeling, we can divide the algorithms into two categories, i.e., non-deep embedding and deep embedding. In [25], the canonical correlation analysis (CCA) [14] is introduced to train the embedding which achieves significant improvement.

Meanwhile, many models [10, 4, 20] construct deep neural networks to map visual feature space to semantic space. They may not directly introduce CNN to learn the embedding, but extract visual feature from original image through CNN. These well-trained deep features usually achieve significant performance.

In particular, graph neural network [9] has recently received great attentions for their flexibility on dealing with graph structures. Inspired by graph convolutional network, the work [34] introduces GNN to transfer visual classifier of seen classes to unseen classes based on a given knowledge graph. However, these methods need to know the correlation between seen and unseen classes which is hard to obtain before training.

In this paper, we utilize the inter-class and intra-class relationship by constructing a heterogeneous graph. Specifically, for each node we use the neighbor information to obtain the embedding result through graph neural network, and then embed unseen class based on the trained embedding model. Compared with previous work in [34], the correlation between all classes need not to be known in advance in our approach which improves its practical utility. The proposed method is inductive. In addition, we simultaneously use the visual features of images as the embedding space to alleviate the hubness problem.

### 3 The Proposed Approach

The goal is to transfer information about the seen classes to unseen classes, and the main obstacle is how to extract and deliver information properly. Our main work is to learn aggregation and embedding functions exactly based on GNN. We also introduce some basic information of Wasserstein barycenter and GNN. The proposed method to deal with zero-shot learning problems by utilizing GNN will be detailed inductively as follows.

#### 3.1 Preliminaries

##### 3.1.1 Notations.

Given a training set  $D_{tr} = \{(x_i, y_i, p_i)\}_{i=1}^N$ , where  $x_i \in \mathbb{R}^n$  is the visual features of  $i$ -th image (here we assume it is extracted by a pretrained network e.g. ResNet [15] which is also a common practice in ZSL literature [36]),  $y_i$  is the label of  $i$ -th image within seen class  $\mathcal{Y}^{tr}$ , i.e.,  $y_i \in \{1, \dots, L\}$ . For each class corresponding to an attribute vector,  $p_i \in \mathbb{R}^d$  is the class prototype of the  $i$ -th image. The goal is to learn a function using  $D_{tr}$  and then predict the label for test visual feature  $x$  within the whole class dictionary  $\mathcal{Y}^t$  including both seen classes  $\mathcal{Y}^{tr}$  and unseen classes  $\mathcal{Y}^{ts}$ , where  $\mathcal{Y}^{tr} \cap \mathcal{Y}^{ts} = \emptyset$ . Moreover,  $\sum_k$  refers to the probability simplex with  $k$  bins, and for two matrices of the same size  $A$  and  $B$ ,  $\langle A, B \rangle := \text{trace}(A^T B)$  is the Frobenius dot-product.  $I$  refers to the identity matrix.

##### 3.1.2 Wasserstein Metric.

Wasserstein metric can be an effective way to measure difference between probability distribution. Given two probabilities  $\mathbf{a}$  and  $\mathbf{b}$  and the non-negative cost matrix  $\mathbf{C}$ , we can define the 1-Wasserstein distance between  $\mathbf{a}$  and  $\mathbf{b}$  as follows:

$$\mathcal{W}_{\mathbf{C}}(\mathbf{a}, \mathbf{b}) := \min_{\mathbf{P} \in \mathcal{U}(\mathbf{a}, \mathbf{b})} \langle \mathbf{P}, \mathbf{C} \rangle, \quad (3.1)$$

where  $\mathbf{P} \in \mathbb{R}^{n \times m}$  is transport matrix, and  $\mathbf{P}_{ij}$  indicates how much mass has moved from position  $i$  to position  $j$ .  $\mathcal{U}(\mathbf{a}, \mathbf{b})$  is the feasible region, which can be defined by:

$$\mathcal{U}(\mathbf{a}, \mathbf{b}) := \{ \mathbf{P} \in \mathbb{R}_+^{n \times m} : \mathbf{P} \mathbf{1}_m = \mathbf{a}, \mathbf{P}^T \mathbf{1}_n = \mathbf{b} \}. \quad (3.2)$$

---

**Algorithm 1** HGKT: Graph Construction  $G(\mathcal{V}, \mathcal{E})$ 

---

**Input:** The set of training data:  $\{D_{tr}\}$ ; the regularization penalty parameters  $\lambda$ ;

- 1: Classify the training data into  $L$ -parts, each part correspond to a class. For each class, connect the node with each other completely;
  - 2: Normalize these data into  $n$ -simplex space  $\sum_n$  and compute the Wasserstein barycenter through (3.3) for each class to get the set of barycenters  $\mathcal{B}$ ;
  - 3: For each class, take the node which is nearest to its barycenter as the representative node, get the set  $\mathcal{S}$  ;
  - 4: For each representative node, select the  $k$ -nearest neighbors in  $\mathcal{S}$  as its neighbors which are connected to the representative node;
  - 5: **return** Adjacency list  $G(\mathcal{V}, \mathcal{E})$ ;
- 

A basic problem in machine learning is to compute the ‘mean’ or ‘barycenter’ of several data points. Based on the above Wasserstein distance, it is natural to introduce the Wasserstein barycenter [1]. Given parameter  $\lambda$  and input histogram  $\{\mathbf{b}_s\}_{s=1}^S$ , where  $\mathbf{b}_s \in \sum_n$ , a Wasserstein barycenter is computed by minimizing

$$\mathcal{WB}(\lambda, \{\mathbf{b}_s\}) = \arg \min_{\mathbf{a} \in \sum_n} \sum_{s=1}^S \lambda_s \mathcal{W}_{\mathbf{C}}(\mathbf{a}, \mathbf{b}_s), \quad (3.3)$$

based on the specified cost matrix  $\mathbf{C} \in \mathbb{R}^{n \times n}$ .

### 3.1.3 Graph Neural Network.

We modify GraphSAGE [13] to solve our problem. The main idea of GraphSAGE is to learn an aggregation function to collect the information of the node’s local neighbors, and learns the embedding function based on the neighbor information. By denoting the learning procedure as function  $g$ , the main goal is to minimize the following empirical risk:

$$\min_{g \in \mathcal{G}} \frac{1}{M} \sum_{m=1}^M \ell(y_m, g(x_m)), \quad (3.4)$$

where  $\ell$  usually denotes the *softmax* loss function, which measures the loss incurred from prediction  $g(x)$  to the true label  $y$ . During testing time, the labels of other  $N-M$  instances are predicted by the obtained function  $g$ .

## 3.2 Heterogeneous Graph Embedding for ZSL

### 3.2.1 Graph Construction.

Inspired by the semi-supervised learning of GraphSAGE, we treat each instance as a node in the graph. For the instances that belong to the same class, they will be connected with each other. As a result, we can obtain  $L$  complete subgraphs. Then the connections between these subgraphs are established.

Now we show our technique for how to select the representative nodes for each class. The node closest to the following obtained Wasserstein barycenter can be an effective means of representing the corresponding class. Specifically for class  $\ell$ , given input visual feature probabilities  $\{x_k\}_{k=1}^{K_\ell}$ , and penalty weights  $\lambda^\ell \in \sum_{K_\ell}$ , the Wasserstein barycenter  $x_\ell$  is computed by  $\mathcal{WB}(\lambda^\ell, \{x_k\})$ .

The representative node  $s_\ell$  for each class can be selected the closest one to the Wasserstein barycenter for each class  $\ell$ :

$$s_\ell = \arg \min_{x_i} \{\mathcal{L}_{\mathbf{C}}(x_\ell, x_i) \mid y_i = \ell\}. \quad (3.5)$$

---

**Algorithm 2** HGKT: Training Procedure

---

**Input:** Graph  $G(\mathcal{V}, \mathcal{E})$ ; Input seen class attributes  $\{p_v\}, \forall v \in \mathcal{V}$ ; Initialization  $\{W_1, W_2\}$ ;  
1:  $h_v^0 \leftarrow p_v, \forall v \in \mathcal{V}$ ;  
2: **for**  $k = 1, 2$  **do**  
3:     **for** each  $v \in \mathcal{V}$  **do**  
4:          $h_{\mathcal{N}(v)}^k \leftarrow \text{Mean}(\{h_u^{k-1}, \forall u \in \mathcal{N}(v)\})$   
5:          $h_v^k \leftarrow \text{Relu}(W_k \cdot \text{CONCAT}(h_v^{k-1}, \mu h_{\mathcal{N}(v)}^k) + b)$   
6:     **end for**  
7: **end for**  
8:  $z_v \leftarrow z_v \cup h_v^2, \forall v \in \text{representative nodes}$   
9: **return** Vector representations  $\{z_v\}$ ;

---

The chosen representative nodes are connected by kNN, thus the whole neighbors of each representative node  $s_\ell$  can be uniformly denoted as

$$\mathcal{N}(s_\ell) = \mathcal{N}_\ell(s_\ell) \cup \mathcal{N}_r(s_\ell), \quad (3.6)$$

where  $\mathcal{N}_\ell$  denotes the neighbors within each class  $\ell$ , and  $\mathcal{N}_r$  denotes the neighbors chosen by using kNN in representative node set. Finally a heterogeneous graph is built, the detailed procedure of graph construction is described in Alg. 1.

### 3.2.2 Training Procedure.

After constructing the heterogeneous graph on training data, we further employ a two-layer GNN scheme for the training procedure. The  $i$ -th node has an attribute vector  $p_i$  and visual feature  $x_i$ .

The attribute vector is used as the initial embedding value for each node  $v$ . Then under the well-established structured graph, the unified neighbor embedding vector of each node  $v$  can be obtained by averaging its neighbors' embedding vectors i.e.,

$$h_{\mathcal{N}(v)} \leftarrow \text{Mean}(\{h_u, \forall u \in \mathcal{N}(v)\}), \quad (3.7)$$

where  $h_{\mathcal{N}(v)}$  denotes the unified neighbor embedding vector of node  $v$ ,  $h_u$  denotes the embedding of node  $u$ .

After aggregation, the unified neighbor embedding vector is concatenated with the original embedding vector of node  $v$ , followed by the embedding procedure:

$$h_v \leftarrow \delta(W \cdot \text{CONCAT}(h_v, \mu h_{\mathcal{N}(v)}) + b), \quad (3.8)$$

where  $h_v$  denotes the embedding vector of node  $v$ ,  $\delta$  denotes the activation function,  $W$  denotes the neural network parameters and  $b$  denotes the bias. Moreover, a regularization parameter  $\mu$  is introduced to balance the importance between unified neighbor embedding vector and original embedding vector. We aim to minimize the distance between the embedding vector and visual feature vector as follows:

$$\text{loss} := \frac{1}{|D_{tr}|} \sum_{i=1}^{|D_{tr}|} \|h(y_i) - x_i\|^2 + \xi \|W\|^2, \quad (3.9)$$

where  $\xi$  denotes the regularization parameter. During training, we can use seen class instances to estimate the parameters. The training procedure is depicted in Alg. 2.

---

**Algorithm 3** HGKT: Testing Procedure

---

**Input:** Graph  $G(\mathcal{V}, \mathcal{E})$ ; All seen class embedding  $\{z_v\}$ ; Input unseen class attributes  $\{\tilde{p}_u\}$ ; test visual feature  $x_t$ ;

- 1: Compute the  $k$ -nearest seen classes for each unseen class and converge them into  $\mathcal{N}(\tilde{p}_u)$ ;
  - 2: Get the embedding result  $\{\tilde{z}_u\}$  by using GNN;
  - 3: For the test visual feature  $x_t$ , choose the nearest embedding’s label within  $\{z_v\} \cup \{\tilde{z}_u\}$  as prediction  $y_t$ ;
  - 4: **return** predict result  $y_t$
- 

### 3.2.3 Testing Procedure.

For seen classes, the embedding vectors have been computed in the train phase. As for new unseen classes, we need to calculate and select  $k$  nearest seen classes as its neighbors, while their embedding vectors can be aggregated directly through the graph and the constructed GNN model. GNN is employed to maintain the topology between classes, as result the relative location of the unseen class can be determined by its neighbor classes. Finally, the visual feature of test samples (could from both seen and unseen classes) are compared with all seen and unseen class embedding vectors, and select the nearest one as its prediction. The detailed procedure of testing is shown in Alg. 3.

## 4 Experiments

### 4.1 Protocols

#### 4.1.1 Datasets.

We select five public benchmark datasets for evaluation, i.e., SUN [24], CUB [32], AwA1 [19], AwA2 [36] and aPY [8]. The detailed setting of the datasets are summarized in Table 2.

#### 4.1.2 Setting.

The same deep features extracted from ResNet-101 [15] and the same attributes presented in [36] are employed in this experiment. The code is implemented in Python and the network is built by Pytorch. The dimension of intermediate layers of our two-layer GNN for five benchmarks are all set to be 1600. The activation layer uses the *leakyRelu* function with slope of 0.2, and ADAM optimizer [17] with a learning rate  $1e^{-4}$  and a weight decay of 0.001 is adopted for training. The regularization parameter  $\mu$  are selected in  $\{0.01, 0.1, 0.5, 1\}$  by validation set. For simplicity, we set the number of neighbors for constructing graph equals to the number of neighbors for unseen classes, and then select  $k$  in  $\{1, 2, 5, 10, 50\}$ . In experiments, the value  $k = 2$  comes up as the best setting.

Moreover, for fairness, we employ the proposed splits (PS) [36] to evaluate the average-class top-1 accuracy on unseen classes  $\mathcal{Y}^{ts}$  and seen classes  $\mathcal{Y}^{tr}$ . In addition the harmonic mean  $H$  of training and test accuracies is used to measure the comprehensive performance of different methods, for both seen and unseen data.

$$H = \frac{2 * acc_{\mathcal{Y}^{tr}} * acc_{\mathcal{Y}^{ts}}}{acc_{\mathcal{Y}^{tr}} + acc_{\mathcal{Y}^{ts}}}. \quad (4.1)$$

#### 4.1.3 Competing Methods.

State-of-the-art methods are selected to compare with our method. Note that [6] and [39] are both agnostic to unseen data, being similar to our approach. However, they use original images instead of extracted features proposed in [36] for model training, the experimental setup of these two algorithms

Table 1: Comparison of GZSL methods on public datasets. Measuring  $ts$  = Top-1 Accuracy on  $\mathcal{Y}^{ts}$ ,  $tr$  = Top-1 Accuracy on  $\mathcal{Y}^{tr}$ ,  $H$  = Harmonic Mean. The result of the compared methods are taken from [36, 20, 4]. Best results are marked in bold.

Dataset	SUN			CUB			AwA1			AwA2			aPY		
Method	$ts$	$tr$	$H$	$ts$	$tr$	$H$	$ts$	$tr$	$H$	$ts$	$tr$	$H$	$ts$	$tr$	$H$
DAP [19]	4.2	25.1	7.2	1.7	67.9	3.3	0.0	<b>88.7</b>	0.0	0.0	84.7	0.0	4.8	78.3	9.0
IAP [19]	1.0	37.8	1.8	0.2	72.8	0.4	2.1	78.2	4.1	0.9	87.6	1.8	5.7	65.6	10.4
CONSE [22]	6.8	39.9	11.6	1.6	72.2	3.1	0.4	88.6	0.8	0.5	<b>90.6</b>	1.0	0.0	<b>91.2</b>	0.0
CMT [29]	8.1	21.8	11.8	7.2	49.8	12.6	0.9	87.6	1.8	0.5	90.0	1.0	1.4	85.2	2.8
CMT* [29]	8.7	28.0	13.3	4.7	60.1	8.7	8.4	86.9	15.3	8.7	89.0	15.9	10.9	74.2	19.0
SSE [38]	2.1	36.4	4.0	8.5	46.9	14.4	7.0	80.5	12.9	8.1	82.5	14.8	0.2	78.9	0.4
LATEM[35]	14.7	28.8	19.5	15.2	57.3	24.0	7.3	71.7	13.3	11.5	77.3	20.0	0.1	73.0	0.2
ALE [2]	21.8	33.1	26.3	23.7	62.8	34.4	16.8	76.1	27.5	14.0	81.8	23.9	4.6	73.7	8.7
DEVISE [10]	16.9	27.4	20.9	23.8	53.0	32.8	13.4	68.7	22.4	17.1	74.7	27.8	4.9	76.9	9.2
SJE [3]	14.7	30.5	19.8	23.5	59.2	33.6	11.3	74.6	19.6	8.0	73.9	14.4	3.7	55.7	6.9
ESZSL [26]	11.0	27.9	15.8	12.6	63.8	21.0	6.6	75.6	12.1	5.9	77.8	11.0	2.4	70.1	4.6
SYNC [5]	7.9	<b>43.4</b>	13.4	11.5	<b>70.9</b>	19.8	8.9	87.3	16.2	10.0	90.5	18.0	7.4	66.3	13.3
SAE [18]	8.8	18.0	11.8	7.8	54.0	13.6	1.8	77.1	3.5	1.1	82.2	2.2	0.4	80.9	0.9
GFZSL [30]	0.0	39.6	0.0	0.0	45.7	0.0	1.8	80.3	3.5	2.5	80.1	4.8	0.0	83.3	0.0
DEM [20]	20.5	34.3	25.6	19.6	57.9	29.2	32.8	84.7	47.3	30.5	86.4	45.1	11.1	75.1	19.4
PSRZSL [4]	20.8	37.2	26.7	24.6	54.3	33.9	-	-	-	20.7	73.8	32.3	13.5	51.4	21.4
HGKT (Ours)	<b>22.3</b>	36.5	<b>27.7</b>	<b>25.2</b>	56.9	<b>34.9</b>	<b>39.4</b>	83.5	<b>53.6</b>	<b>37.9</b>	86.5	<b>52.7</b>	<b>18.3</b>	79.0	<b>29.7</b>

Table 2: Benchmark datasets.  $\mathcal{Y}^{tr}$  and  $\mathcal{Y}^{ts}$  represent the seen class and the unseen class respectively.

Dataset	Class Number			Number of Images			
	Attribute	$\mathcal{Y}^{tr}$	$\mathcal{Y}^{ts}$	Training Set		Test Set	
				$\mathcal{Y}^{tr}$	$\mathcal{Y}^{ts}$	$\mathcal{Y}^{tr}$	$\mathcal{Y}^{ts}$
SUN	102	645	72	10320	0	2580	1440
CUB	312	150	50	7057	0	1764	2967
AwA1	85	40	10	19832	0	4958	5685
AwA2	85	40	10	23527	0	5882	7913
aPY	64	20	12	5932	0	1483	7924

is different from ours. Moreover, the method in [39] need to decompose an image into visual parts, but images in some datasets like SUN cannot be easily decomposed as they are often compact and consistent across different scenes. Thus in the corresponding experiment, we do not take these two methods into account.

## 4.2 Results and Discussion

### 4.2.1 Overall Comparison with Peer Methods

We first make a comparison with state-of-the-arts for conventional ZSL which only consider unseen classes at test time. The results are listed in Table 3. Compared to the baseline DEM, our proposed method outperforms in all benchmark datasets. Moreover, we achieve the state-of-the-art in SUN, AwA1, AwA2, aPY datasets. In particular, our result is further improved to 68.9% in AwA2 dataset, which is 5.1% higher than the best result reported so far. Despite we obtain 54.2% on CUB dataset which is slightly less than PSRZSL, our approach HGKT performs much better on the generalized zero-shot setting, as illustrated next.

For GZSL, the evaluation results are listed in Table 1. Note that our approach obtains the highest top-1 accuracy of  $H$  and unseen classes on all datasets. For AwA1, AwA2 and aPY datasets, our method improves the top-1 accuracy by a high margin. Especially, compared to the key baseline



Table 3: Average per-class accuracy for conventional ZSL.

Method	SUN	CUB	AwA1	AwA2	aPY
DAP [19]	39.9	40.0	44.1	46.1	33.8
IAP [19]	19.4	24.0	35.9	35.9	36.6
CONSE [22]	38.8	34.3	45.6	44.5	26.9
CMT [29]	39.9	34.6	39.5	37.9	28.0
SSE [38]	51.5	43.9	60.1	61.0	34.0
LATEM [35]	55.3	49.3	55.1	55.8	35.2
ALE [2]	58.1	54.9	59.9	62.5	39.7
DEVISE [10]	56.5	52.0	54.2	59.7	39.8
SJE [3]	53.7	53.9	65.6	61.9	32.9
ESZSL [26]	54.5	53.9	58.2	58.6	38.3
SYNC [5]	56.3	55.6	54.0	46.6	23.9
SAE [18]	40.3	33.3	53.0	54.1	8.3
GFZSL [30]	60.6	49.3	68.3	63.8	38.4
DEM [20]	61.9	50.1	64.2	61.9	34.5
PSRZSL [4]	61.4	<b>56.0</b>	-	63.8	38.4
HGKT (ours)	<b>62.1</b>	54.2	<b>69.1</b>	<b>68.9</b>	<b>41.5</b>

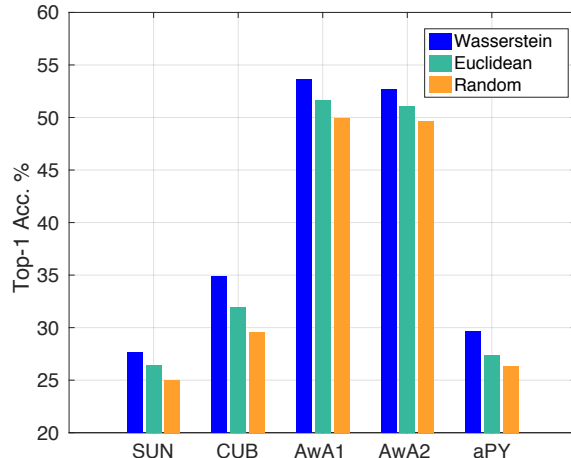


Figure 3: Harmonic mean of three node selecting methods.

DEM method, our method gains 10.3%, 6.3% and 7.6% improvement on aPY, AwA1 and AwA2 datasets respectively. Compared to the state-of-art approach PSRZSL [4], which relies on using semantic relations to learn the embedding, our algorithm can improve prominently 20.4% on AwA2 datasets. It can be seen that our method improves the accuracy of unseen classes notably, which usually dominates the harmonic mean  $H$ . Moreover, we also count Table 1 about seen classes, unseen classes and  $H$  in Fig. 7, which further illustrates the effectiveness of our approach.

In fact, existing algorithms like DAP, CONSE and SYNC often achieve competitive results on seen classes, while poorly on unseen classes. These methods almost only consider seen classes like the one for traditional image classification, but the most important problem in ZSL is how to generalize seen classes to unseen classes, so these methods have limitations in this regard.

To illustrate the effectiveness of our method, we use the dataset AwA2 to visualize (by t-SNE [21]) the embedding for unseen classes. As shown in Fig. 4, visual features of each unseen class are well separated from each other. We use black circles to indicate the embedding of unseen classes, and it is obvious that our approach embeds 80% unseen classes into their own clusters. In contrast,

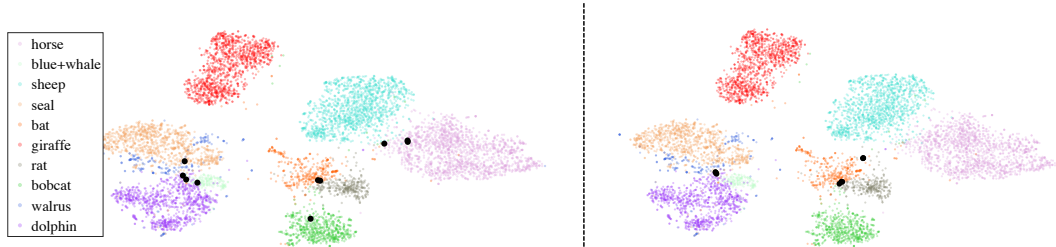


Figure 4: T-SNE visualization of the distribution of the ten unseen classes on Awa2. Black dots denote the embedding vectors for unseen classes obtained by different methods. Left: embedding vectors by our method; right: by the baseline DEM.

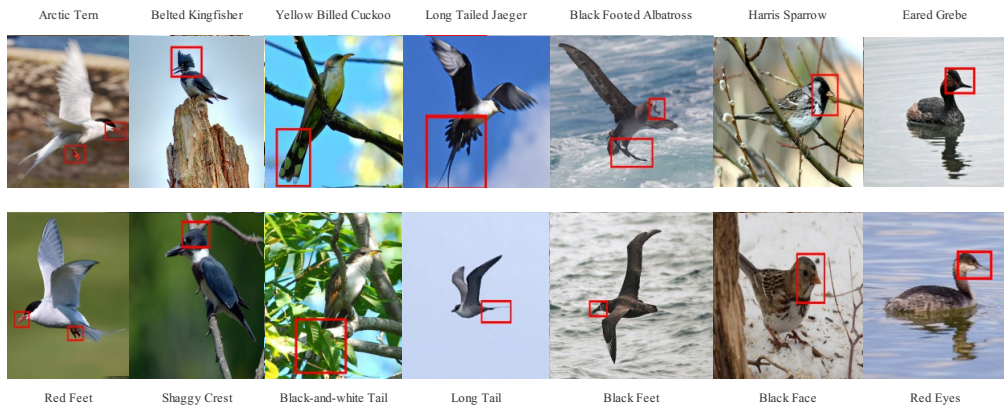


Figure 5: Representative images selected by Wasserstein barycenter (top) and Euclidean barycenter (bottom) on CUB dataset.

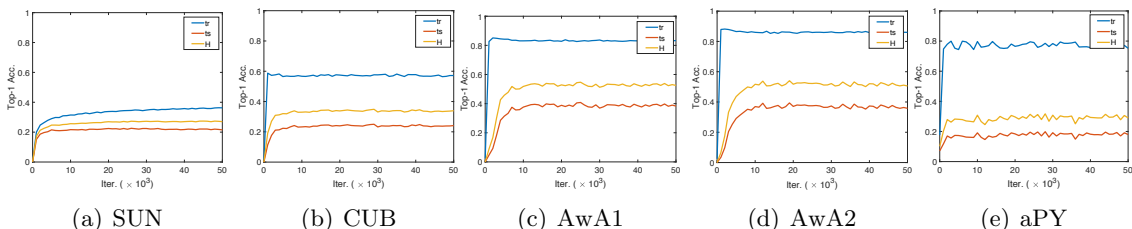


Figure 6: Testing accuracy against number of iterations on the tested five public datasets.

the baseline DEM embed much fewer. DEM has difficulty in distinguishing the embedding between adjacent unseen classes, and as a result these embedding will gather together. By contrast, our algorithm can utilize neighbors to pull the embedding in different directions and separate them.

#### 4.2.2 Effectiveness of intra-class relationship.

The aim of this study is to determine the effect of constructing complete-graph. On the left of Table 4, we find that without constructing complete-graph for each class, the results are lower than ones that do it. This indicates that construct intra-class relationship can improve result.

#### 4.2.3 Effectiveness of inter-class relationship.

We also evaluate our algorithm without constructing inter-class relationship. On the right of Table 4, we observe that constructing inter-class relationship outperforms the ‘none’ by a large margin. In

Table 4: Effect of intra-class and inter-class relationship on five benchmarks, CG refer to the complete graph.

Dataset	Intra-class	$ts$	$tr$	$H$	Inter-class	$ts$	$tr$	$H$
SUN	None	22.2	33.4	26.7	None	21.5	32.5	25.9
	CG	22.3	36.5	<b>27.7</b>	kNN	22.3	36.5	<b>27.7</b>
CUB	None	24.4	56.7	34.1	None	23.0	56.6	32.7
	CG	25.2	56.9	<b>34.9</b>	kNN	25.2	56.9	<b>34.9</b>
AwA1	None	34.9	82.6	49.1	None	32.6	84.0	46.9
	CG	39.4	83.5	<b>53.6</b>	kNN	39.4	83.5	<b>53.6</b>
AwA2	None	36.1	85.5	50.7	None	25.7	86.5	39.6
	CG	37.9	86.5	<b>52.7</b>	kNN	37.9	86.5	<b>52.7</b>
aPY	None	14.3	56.7	22.8	None	13.1	76.3	22.4
	CG	18.3	79.0	<b>29.7</b>	kNN	18.3	79.0	<b>29.7</b>

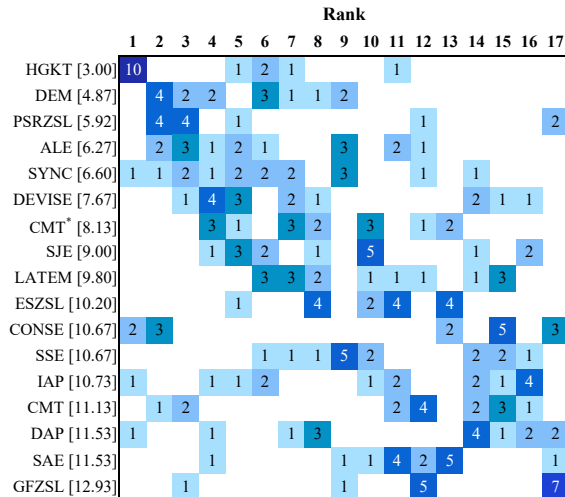


Figure 7: Statistic about the value of  $ts$ ,  $tr$  and  $H$  in Table 1. Element  $(i, j)$  indicates number of times model  $i$  ranks at  $j$ th over all  $5 \times 3$  columns. Models are ordered by their mean rank (displayed in brackets).

particular, for AwA2 dataset, the accuracy increases from 39.6% to 52.7%. These results show that our model can transfer knowledge from seen classes efficiently.

#### 4.2.4 Effectiveness of Wasserstein metric.

We perform ablation study to the efficiency of different node selection methods in our approach. Besides the Wasserstein barycenter, we can also select representative nodes by Euclidean barycenter (averaging directly) and random number. As shown in Fig. 3, the Wasserstein barycenter outperforms the others. It is obvious that selecting representative nodes randomly usually causes a significant drop in accuracy, for the reason that the resulting representative node is more likely to fall into the overlap, thus it is prone to classify images into wrong class by using kNN during testing. Moreover, by visualizing these representative nodes selected by different techniques in Fig. 5, we can find that intuitively the nodes selected by Wasserstein distance have more distinctive features.

**Convergence and Scalability.** The accuracy on the test set against the number of iterations for the five benchmark datasets is shown in Fig. 6. It is also noteworthy that our approach can quickly converge to the final results on all datasets. In addition, in order to address the scalability issues, we uniformly sample a fixed-set of neighbors  $S$ , instead of using full neighborhood sets during training.

In addition, because the depth of our algorithm is 2, thus the per-batch time complexity is fixed at  $O(S^2)$ . In experiments, we set  $S$  equals to 50.

Moreover, due to the large amount of data, we choose Sinkhorn distance [7] to compute an approximate Wasserstein barycenter, which also possess the scalability problem. Specifically, the penalty weight for each instance is set to be same, the cost matrix  $C$  is set to be  $C_{ij} = \|i - j\|_2^2$  and the parameter  $\epsilon$  in Sinkhorn is set to be  $1e^{-5}$ , while guarantees estimated good enough results.

## 5 Conclusion

We have presented a heterogeneous graph-based model for GZSL. Unlike most existing algorithms, our method is agnostic to test data during training, which makes our approach can adapt to the dynamic scenarios effectively. We construct a meaningful structured graph to represent the relation among the data. Instead of Euclidean space, our experiments show that constructing graph in Wasserstein space can achieve better results. Further the graph neural network can be employed to train our model on the well-constructed graph. Extensive experimental results show that more explainable embedding can be obtained for unseen classes which leads to higher top-1 accuracy compared to peer methods.

## References

- [1] Martial Agueh and Guillaume Carlier. Barycenters in the wasserstein space. *SIAM Journal on Mathematical Analysis*, 43(2):904–924, 2011.
- [2] Zeynep Akata, Florent Perronnin, Zaid Harchaoui, and Cordelia Schmid. Label-embedding for image classification. *IEEE Transactions on Pattern Analysis and Machine Intelligence*, 38(7):1425–1438, 2016.
- [3] Zeynep Akata, Scott Reed, Daniel Walter, Honglak Lee, and Bernt Schiele. Evaluation of output embeddings for fine-grained image classification. In *CVPR*, pages 2927–2936, 2015.
- [4] Yashas Annadani and Soma Biswas. Preserving semantic relations for zero-shot learning. In *CVPR*, pages 7603–7612, 2018.
- [5] Soravit Changpinyo, Wei-Lun Chao, Boqing Gong, and Fei Sha. Synthesized classifiers for zero-shot learning. In *CVPR*, pages 5327–5336, 2016.
- [6] Long Chen, Hanwang Zhang, Jun Xiao, Wei Liu, and Shih-Fu Chang. Zero-shot visual recognition using semantics-preserving adversarial embedding networks. In *CVPR*, pages 1043–1052, 2018.
- [7] Marco Cuturi. Sinkhorn distances: Lightspeed computation of optimal transport. In *NeurIPS*, pages 2292–2300, 2013.
- [8] Ali Farhadi, Ian Endres, Derek Hoiem, and David Forsyth. Describing objects by their attributes. In *CVPR*, pages 1778–1785, 2009.
- [9] Scarselli Franco, Gori Marco, Tsoi Ah Chung, Hagenbuchner Markus, and Monfardini Gabriele. The graph neural network model. *IEEE Transactions on Neural Networks*, 20(1):61–80, 2009.
- [10] Andrea Frome, Greg S Corrado, Jon Shlens, Samy Bengio, Jeff Dean, Tomas Mikolov, et al. Devise: A deep visual-semantic embedding model. In *NeurIPS*, pages 2121–2129, 2013.
- [11] Yanwei Fu, Tao Xiang, Yu-Gang Jiang, Xiangyang Xue, Leonid Sigal, and Shaogang Gong. Recent advances in zero-shot recognition: Toward data-efficient understanding of visual content. *IEEE Signal Processing Magazine*, 35(1):112–125, 2018.
- [12] Ian Goodfellow, Jean Pouget-Abadie, Mehdi Mirza, Bing Xu, David Warde-Farley, Sherjil Ozair, Aaron Courville, and Yoshua Bengio. Generative adversarial nets. In *NeurIPS*, pages 2672–2680, 2014.
- [13] Will Hamilton, Zhitao Ying, and Jure Leskovec. Inductive representation learning on large graphs. In *NeurIPS*, pages 1024–1034, 2017.

- [14] David R Hardoon, Sandor Szedmak, and John Shawe-Taylor. Canonical correlation analysis: An overview with application to learning methods. *Neural Computation*, 16(12):2639–2664, 2004.
- [15] Kaiming He, Xiangyu Zhang, Shaoqing Ren, and Jian Sun. Deep residual learning for image recognition. In *CVPR*, pages 770–778, 2016.
- [16] Michael Kampffmeyer, Yinbo Chen, Xiaodan Liang, Hao Wang, Yujia Zhang, and Eric P Xing. Rethinking knowledge graph propagation for zero-shot learning. In *CVPR*, pages 11487–11496, 2019.
- [17] Diederik P Kingma and Jimmy Ba. Adam: A method for stochastic optimization. In *ICLR*, 2015.
- [18] Elyor Kodirov, Tao Xiang, and Shaogang Gong. Semantic autoencoder for zero-shot learning. In *CVPR*, pages 3174–3183, 2017.
- [19] Christoph H Lampert, Hannes Nickisch, and Stefan Harmeling. Attribute-based classification for zero-shot visual object categorization. *IEEE Transactions on Pattern Analysis and Machine Intelligence*, 36(3):453–465, 2014.
- [20] Zhang Li, Xiang Tao, and Shaogang Gong. Learning a deep embedding model for zero-shot learning. In *CVPR*, pages 2021–2030, 2017.
- [21] Laurens van der Maaten and Geoffrey Hinton. Visualizing data using t-SNE. *Journal of Machine Learning Research*, 9(Nov):2579–2605, 2008.
- [22] Mohammad Norouzi, Tomas Mikolov, Samy Bengio, Yoram Singer, Jonathon Shlens, Andrea Frome, Greg S Corrado, and Jeffrey Dean. Zero-shot learning by convex combination of semantic embeddings. In *ICLR*, 2014.
- [23] Mark Palatucci, Dean Pomerleau, Geoffrey E Hinton, and Tom M Mitchell. Zero-shot learning with semantic output codes. In *NeurIPS*, pages 1410–1418, 2009.
- [24] Genevieve Patterson and James Hays. Sun attribute database: Discovering, annotating, and recognizing scene attributes. In *CVPR*, pages 2751–2758, 2012.
- [25] Guo-Jun Qi, Wei Liu, Charu Aggarwal, and Thomas Huang. Joint intermodal and intramodal label transfers for extremely rare or unseen classes. *IEEE Transactions on Pattern Analysis and Machine Intelligence*, 39(7):1360–1373, 2017.
- [26] Bernardino Romera-Paredes and Philip Torr. An embarrassingly simple approach to zero-shot learning. In *ICML*, pages 2152–2161, 2015.
- [27] Yutaro Shigeto, Ikumi Suzuki, Kazuo Hara, Masashi Shimbo, and Yuji Matsumoto. Ridge regression, hubness, and zero-shot learning. In *ECML/PKDD*, pages 135–151, 2015.
- [28] Jake Snell, Kevin Swersky, and Richard Zemel. Prototypical networks for few-shot learning. In *NeurIPS*, pages 4077–4087, 2017.
- [29] Richard Socher, Milind Ganjoo, Christopher D Manning, and Andrew Ng. Zero-shot learning through cross-modal transfer. In *NeurIPS*, pages 935–943, 2013.
- [30] Vinay Kumar Verma and Piyush Rai. A simple exponential family framework for zero-shot learning. In *ECML-PKDD*, pages 792–808, 2017.
- [31] Cédric Villani. *Optimal transport: old and new*, volume 338. Springer Science & Business Media, 2008.
- [32] C. Wah, S. Branson, P. Welinder, P. Perona, and S. Belongie. The Caltech-UCSD Birds-200-2011 Dataset. Technical Report CNS-TR-2011-001, California Institute of Technology, 2011.
- [33] Wei Wang, Vincent W Zheng, Han Yu, and Chunyan Miao. A survey of zero-shot learning: Settings, methods, and applications. *ACM Transactions on Intelligent Systems and Technology*, 10(2):13, 2019.
- [34] Xiaolong Wang, Yufei Ye, and Abhinav Gupta. Zero-shot recognition via semantic embeddings and knowledge graphs. In *CVPR*, pages 6857–6866, 2018.
- [35] Yongqin Xian, Zeynep Akata, Gaurav Sharma, Quynh Nguyen, Matthias Hein, and Bernt Schiele. Latent embeddings for zero-shot classification. In *CVPR*, pages 69–77, 2016.

- [36] Yongqin Xian, Christoph H Lampert, Bernt Schiele, and Zeynep Akata. Zero-shot learning-a comprehensive evaluation of the good, the bad and the ugly. *IEEE Transactions on Pattern Analysis and Machine Intelligence*, 41(9):2251–2265, 2019.
- [37] Gang Yang, Jinlu Liu, Jieping Xu, and Xirong Li. Dissimilarity representation learning for generalized zero-shot recognition. In *ACM Multimedia*, pages 2032–2039, 2018.
- [38] Ziming Zhang and Venkatesh Saligrama. Zero-shot learning via semantic similarity embedding. In *ICCV*, pages 4166–4174, 2015.
- [39] Pengkai Zhu, Hanxiao Wang, and Venkatesh Saligrama. Generalized zero-shot recognition based on visually semantic embedding. In *CVPR*, pages 2995–3003, 2019.